Molecular Therapy
Methods & Clinical Development
Original Article

CERE-120 Prevents Irradiation-Induced Hypofunction and Restores Immune Homeostasis in Porcine Salivary Glands

Isabelle M.A. Lombaert,[1,2,3,11] Vaishali N. Patel,[1,11] Christina E. Jones,[1] Derrick C. Villier,[1] Ashley E. Canada,[1] Matthew R. Moore,[1] Elsa Berenstein,[1] Changyu Zheng,[4] Corinne M. Goldsmith,[4] John A. Chorini,[5] Daniel Martin,[6] Lee Zourelias,[7] Mark G. Trombetta,[8] Paul C. Edwards,[9] Kathleen Meyer,[10] Dale Ando,[10] Michael J. Passineau,[7] and Matthew P. Hoffman[1]

[1]Matrix and Morphogenesis Section, National Institute of Dental and Craniofacial Research, NIH, DHHS, Bethesda, MD 20892, USA; [2]Department of Biologic and Materials Sciences, School of Dentistry, University of Michigan, Ann Arbor, MI 48109, USA; [3]Biointerfaces Institute, University of Michigan, Ann Arbor, MI 48109, USA; [4]Translational Research Core, NIDCR, NIH, DHHS, Bethesda, MD 20892, USA; [5]Adeno-Associated Virus Section, NIDCR, NIH, DHHS, Bethesda, MD 20892, USA; [6]Genomics and Computational Biology Core, NIDCR, NIH, DHHS, Bethesda, MD 20892, USA; [7]Gene Therapy Program, Department of Medicine, Division of Cardiovascular Medicine, Allegheny Health Network, Pittsburg, PA 15212, USA; [8]Department of Oncology, Division of Radiation Oncology, Allegheny Health Network, Pittsburg, PA 15212, USA; [9]Department of Oral Pathology, Medicine, and Radiology, Indiana University School of Dentistry, Indianapolis, IN 46202, USA; [10]Sangamo BioSciences, Inc., 501 Canal Blvd., Richmond, CA 94804

Salivary gland hypofunction causes significant morbidity and loss of quality of life for head and neck cancer patients treated with radiotherapy. Preventing hypofunction is an unmet therapeutic need. We used an adeno-associated virus serotype 2 (AAV2) vector expressing the human neurotrophic factor neurturin (CERE-120) to treat murine submandibular glands either pre- or post-irradiation (IR). Treatment with CERE-120 pre-IR, not post-IR, prevented hypofunction. RNA sequencing (RNA-seq) analysis showed reduced gene expression associated with fibrosis and the innate and humoral immune responses. We then used a minipig model with CERE-120 treatment pre-IR and also compared outcomes of the contralateral non-IR gland. Analysis of gene expression, morphology, and immunostaining showed reduced IR-related immune responses and improved secretory mechanisms. CERE-120 prevented IR-induced hypofunction and restored immune homeostasis, and there was a coordinated contralateral gland response to either damage or treatment. CERE-120 gene therapy is a potential treatment for head and neck cancer patients to influence communication among neuronal, immune, and epithelial cells to prevent IR-induced salivary hypofunction and restore immune homeostasis.

INTRODUCTION

Every year over 500,000 head and neck cancer (HNC) patients worldwide receive radiotherapy treatment. A major complication is irreversible salivary gland hypofunction, due to the location of the glands in the radiation field.[1] Salivary hypofunction is associated with increased oral and dental diseases, speech impairment, loss of taste, and dysphagia, negatively impacting the patient's quality of life. Current therapies are palliative, but recent experimental approaches to restore function involve drugs affecting mammalian target of rapamycin (mTOR) signaling,[2,3] stem cell therapies to repair and/or regenerate functional tissue,[4,5] and gene therapy to increase salivary function using viral vectors expressing aquaporins, which is currently in human clinical trials.[6,7]

Exocrine glands, such as salivary and lacrimal glands, are highly innervated and depend on the autonomic nervous system for proper development, homeostasis, and functional regeneration after injury.[8–11] Analysis of both human and murine submandibular glands (SMGs) treated with irradiation (IR) show that epithelial-neuronal bidirectional communication is impacted. Although neurons are considered relatively IR-resistant, both mouse and human adult salivary glands damaged by IR have reduced parasympathetic innervation and a resulting imbalance of sympathetic innervation.[9] Saliva secretion requires innervation, so we used a neurotrophic factor, neurturin (NRTN), to prevent IR-induced hypofunction by preserving innervation. NRTN is mainly secreted by epithelial cells and is essential for parasympathetic neuronal survival and axon growth.[9,12] Not surprisingly, mice with genetic deletion of either *Nrtn* or its receptor *Gfrα2* have fewer parasympathetic neurons and reduced salivary gland innervation and function.[13,14]

Previously, we used an adenovirus serotype 5 vector expressing human NRTN delivered to murine SMGs 24 h before IR and analyzed

Received 7 March 2020; accepted 27 July 2020;
https://doi.org/10.1016/j.omtm.2020.07.016.

[11]These authors contributed equally to this work.

Correspondence: Matthew P. Hoffman, BDS, PhD, Matrix and Morphogenesis Section, National Institute of Dental and Craniofacial Research, NIH, DHHS, Bethesda, MD 20892, USA.
E-mail: mhoffman@nih.gov

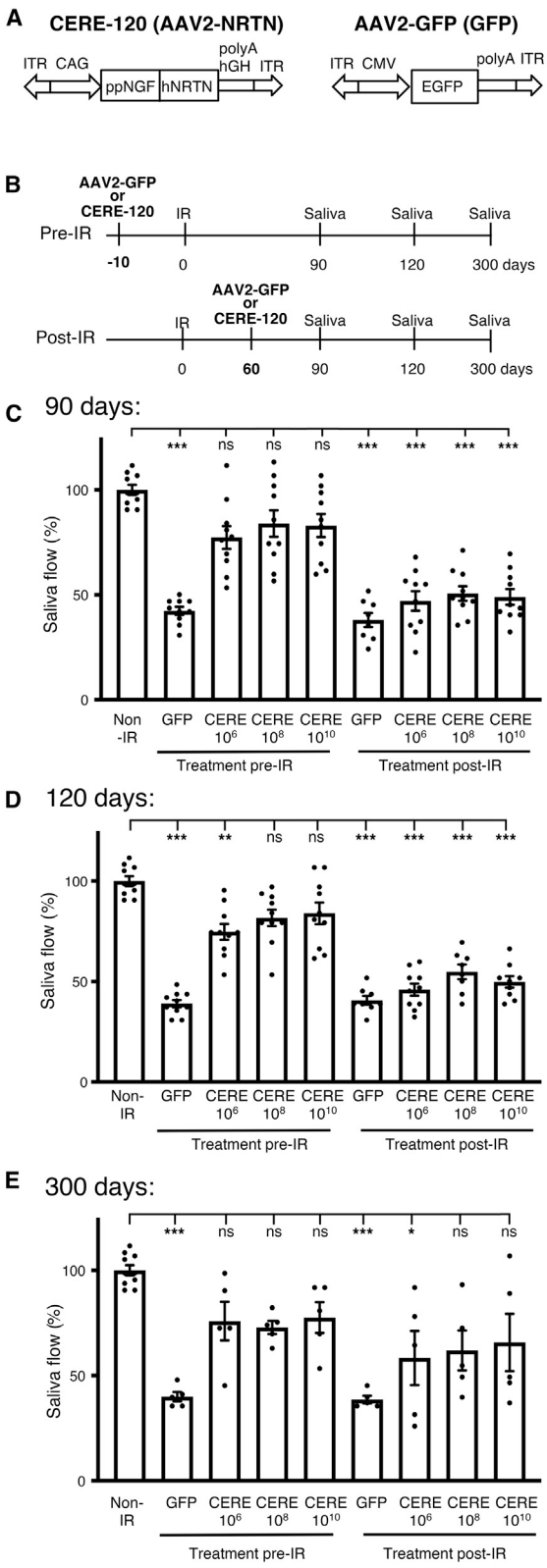

Figure 1. CERE-120 Treatment Pre-IR, as Compared to Post-IR, Prevents Long-Term Hyposalivation in Murine SMGs.

(A) Structure of the CERE-120 vector and the AAV2-GFP vector. (B) Schematic illustration showing the two arms of the mouse study design. (C–E) Pilocarpine-stimulated whole saliva was measured at 90 (C), 120 (D), or 300 (E) days post-IR in AAV2-GFP (10^{10} vp/g) or CERE-120 (10^6, 10^8, and 10^{10} vp/g)-treated animals and compared to non-IR mice (baseline). Saliva flow normalized to non-IR and shown as %. Mean ± SEM. N = 5–10 mice. Dots represent saliva measurements of individual mice. ANOVA with *post hoc* Dunnett's test, ***p < 0.001; **p < 0.01, *p < 0.05, not significant (ns) compared to non-IR.

gene expression 60 days later. The NRTN-treated glands had a similar flow to non-irradiated (non-IR) glands, and expression of neuronal markers, such as *Ret*, *Tubb3*, *Vacht*, and *Th*, increased, suggesting that NRTN gene therapy may prevent IR-induced hypofunction.[8] To advance this therapy toward the clinic, we needed to change the viral vector to an adeno-associated virus serotype 2 (AAV2), which has longer expression and fewer immune side effects and is now the vector of choice for the current AAV2-AQP1 gene therapy clinical trial[7] (ClinicalTrials.gov: NCT02446249). Here, we used an AAV2-based vector encoding human NRTN (CERE-120), which was made by Ceregene, a part of Sangamo BioSciences. CERE-120 has been used in humans in clinical trials for Parkinson's disease (ClinicalTrials.gov: NCT00252850 and NCT00400634).[15,16] We tested CERE-120 in mice pre- and post-IR and used RNA-seq analysis to identify changes in gene expression. We moved to a large animal porcine model, in which we could IR and treat only one parotid gland (PG) but analyze saliva flow separately from the IR and contralateral gland over time. The porcine PG is a translational model, used for preclinical studies of efficacy and/or safety of drug and gene therapies.[3,17–20] Porcine PGs respond to IR in a similar manner to human glands, in terms of gland anatomy, physiology, and the fibrotic and inflammatory responses to IR.[21] Together, our studies show that CERE-120 may be an effective preventative gene therapy approach to reduce salivary hypofunction by increasing innervation of the gland, restoring immune homeostasis, and reducing the fibrotic response to injury in submandibular and parotid salivary glands.

RESULTS

Gene Therapy with CERE-120 Treatment Pre-IR, as Compared to Post-IR, Prevents Long-Term Hyposalivation in Murine SMGs

CERE-120 has coding sequences essential for replication removed to generate a vector with only the non-coding inverted terminal repeats (ITRs) of the AAV2 (Figure 1A).[15] CERE-120 is an AAV2 vector that consists of a CAG promoter replacing the coding sequences, a cDNA region encoding the β-nerve growth factor pre-pro region (ppNGF) fused to the mature region of human NRTN (hNRTN), and a polyA sequence from human growth hormone (hGH). A panel of various constructs generated the CAG promoter: a human cytomegalovirus (CMV) enhancer, a chicken β-actin promoter and splice donor, and a rabbit α-globin splice acceptor. The ppNGF promotes optimal processing and secretion of hNRTN. As a control, an AAV2-GFP vector, which contains both AAV serotype 2 Capsid and ITR, and expresses EGFP under the control of a CMV promoter, was purchased from Vector Biolabs.

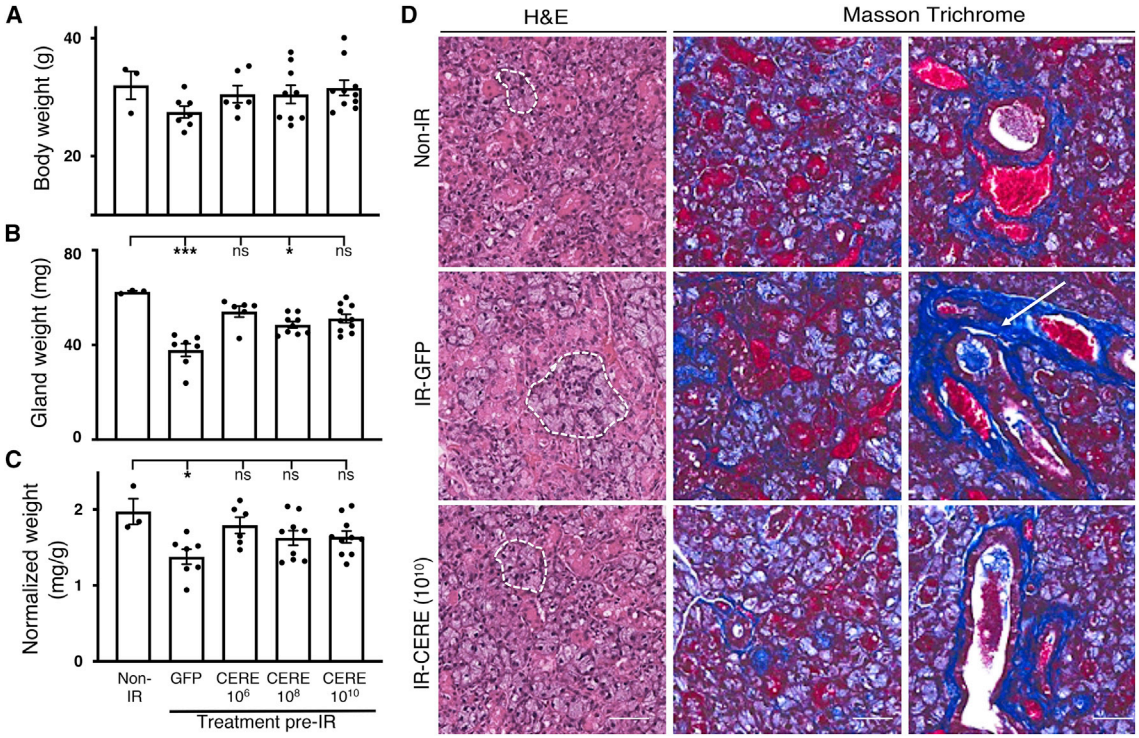

Figure 2. Gland Anatomy and Morphology Improves after CERE-120 Pre-IR Treatment.

(A–C) Analysis of the body weight (g) (A), submandibular gland weight (mg), (B) and normalized ratio of gland weight to body weight (mg/g) (C) at 300 days of non-IR mice, and mice treated with AAV2-GFP (10^{10} vp/g) or CERE-120 (10^6, 10^8, and 10^{10} vp/g) pre-IR. Dots represent measurement of individual mice. Mean ± SEM. N = 3–10 mice. ANOVA with *post hoc* Dunnett's test, ***$p < 0.001$, *$p < 0.05$, not significant (ns) as compared to non-IR. (D) H&E and Masson's trichrome (MT) staining of SMGs of non-IR mice, and mice treated with AAV2-GFP (10^{10} vp/g) or CERE-120 (10^{10} vp/g) pre-IR. Images are representative of results from N ≥ 3 mice. Scale bar, 50 μm.

As AAV vectors in the salivary gland are reported to have slow kinetics of expression but result in prolonged expression,[22] we treated the murine glands with AAV2 10 days pre-IR (Figure 1B). For the post-IR treatment groups, we used the treatment time frame that had been used for murine experiments with AAV2-AQP1, which was treatment 60 days post-IR when salivary flow was reduced.[23] The CERE-120 (10^6, 10^8, or 10^{10} viral particles/gland [vp/g]) or AAV2-GFP (10^{10} vp/g) vectors were administered by retro-ductal infusion into SMGs at 60 days post-IR. A fractionated IR dose (6 × 5 Gy) was used to induce hyposalivation,[8] which was measured by pilocarpine stimulation of whole saliva production. Saliva was collected 90 days post-IR, and the IR control group produced ~65% less saliva compared to the non-IR group (baseline), irrespective of whether the AAV2-GFP was delivered pre- or post-IR (Figures 1C–1E). All CERE-120 treatments pre-IR (10^6, 10^8, 10^{10} vp/g) resulted in improved saliva flow compared to the IR-GFP group and were similar to the non-IR group at 90 and 300 days. At 120 days, there were differences in the 3 doses with CERE-120 at 10^8 and 10^{10} vp/g being similar to non-IR. In comparison, CERE-120 post-IR treatment groups only showed similar saliva flow to the non-IR group at 300 days, not at 90 and 120 days post-IR (Figures 1C and 1D). At 300 days, the post-IR-treated groups had more variability in their response, although 4 of the 15 individual mice in the 3 groups (10^6, 10^8, 10^{10} vp/g) showed saliva levels similar to the non-IR group. Further study is required to investigate what may be causing the variation in response to treatment post-IR treatment.

Gland Anatomy and Morphology Improves after CERE-120 Treatment Pre-IR

The body weights of mice from all treatment groups were similar to the control (Figure 2A). IR treatment can reduce salivary gland weight in animal models of irradiation.[21] Accordingly, the SMG weights of IR-GFP animals and the CERE-120 (10^8) group were reduced compared to the non-IR group (Figure 2B), whereas the SMG weights of CERE-120 (10^6 and 10^{10}) groups were similar to non-IR SMGs. When the gland weight was normalized to body weight, only the IR-GFP group was reduced compared to the non-IR group, and all doses of CERE-120 were similar to the non-IR group (Figure 2C).

In this IR-mouse model,[24–26] IR-induced hyposalivation occurs without a major loss in saliva-producing acinar cells. However, these acinar cells do not function correctly, and in physiology experiments of these IR cells the rate and extent of acinar cell volume decrease upon stimulation of secretion is reduced.[26] Histologically, this corresponds to the appearance of large acinar cell clusters[26] (Figure 2D; Figure S1A, dotted line) in IR and AAV2-GFP-treated glands.

Interestingly, these large acinar clusters were not observed in IR-CERE-treated mice, and many acini appeared similar in size to non-IR glands. With fibrosis being a long-term side effect of IR, AAV2-GFP glands also had large areas of periductal and perivascular fibrosis, with collagen-rich connective tissue bundles appearing dark blue with Masson's trichrome (MT) staining (Figure 2D, arrow). In IR-CERE-treated glands, there appeared to be fewer collagen-rich tissue fibers than IR-GFP-treated glands and a similar number of fibers along ducts and blood vessels comparable to non-IR glands. Taken together, the data suggest that pre-IR treatment with CERE-120 improves the weight of the gland and reduces the appearance of periductal fibrosis.

RNA Sequencing Analysis Shows that CERE-120 Treatment Pre-IR Reduces the Expression of Genes Related to IR-Induced Fibrosis and the Innate and Adaptive Humoral Immune Responses

In order to investigate the transcriptional changes that occur with CERE-120 treatment, we used RNA sequencing (RNA-seq) to compare non-IR SMGs with both IR SMGs treated with AAV2-GFP (IR-GFP) or CERE-120 (IR-CERE, 10^8 vg/g). By assigning a nominal significance level of 0.05 and a log fold change of ≥ 2, we identified 72 differentially expressed genes (DEGs) between non-IR and IR-GFP-treated glands (Table 1). There were 31 DEGs upregulated and 41 downregulated. We used qPCR to confirm some of the gene expression changes from the RNA-seq data (Figure 3A). Examples of DEGs that were upregulated after IR-GFP are genes involved in matrix deposition, such as a collagen (*Col23a1*); matrix metalloproteinases (MMPs) involved in extracellular matrix (ECM) remodeling (*Mmp2*, *Mmp3*);[27] a cysteine peptidase inhibitor involved in ECM remodeling and fibrosis (*Serping1*);[28,29] and injury-associated phospholipase enzyme involved in epidermal growth factor receptor (EGFR) signaling (*Pla1a*)[30] (Figure 3A). Other upregulated genes are related to inflammation and immune function (*Clec12a*, *Cma1*, *Pld4*, *Lyz2*). A general observation was that treatment with CERE-120 (IR-CERE) reduced gene expression to similar levels as the non-IR group (Figure 3A). We also confirmed the downregulation of genes by qPCR, for example, a neuronal voltage gated Na channel (*Scn3a*); epidermal growth factor (*Egf*), which is expressed by epithelial granular ducts; and an epithelial semaphorin gene (*Sema3c*), potentially involved in regulating innervation. As expected, acinar cell genes related to salivary secretion, such as the embryonic form of mucin 19 (*Smgc*), amylase (*Amy1*, a salivary enzyme), and secernin (*Scrn1*, a gene involved in exocytosis), were also reduced with IR-GFP treatment. Another general observation was that treatment with CERE-120 (IR-CERE) increased gene expression to levels similar to the non-IR group. An exception in our qPCR analyses was amylase (*Amy1*), a secreted enzyme that did not increase with CERE-120 treatment, and, as expected, E-cadherin (*Cdh1*), which is highly expressed in epithelial ducts, was not affected.

By comparing the RNA-seq data from IR-GFP with IR-CERE treatment groups after 300 days post-IR, surprisingly, we only observed 38 DEGs (Table 2). There were 3 DEGs upregulated and 35 downregulated with CERE-120 treatment. These are interesting genes, because they potentially highlight the secondary effects of CERE-120 in an irradiated microenvironment. There was a striking reduction of immunoglobulin gene expression (9 out of 37 genes were immunoglobulins [Igs]), suggesting that CERE-120 treatment reduces or resolves humoral immune response to IR. We speculate that CERE-120 helps restore immune homeostasis in the gland. Further supporting this speculation, there was reduced expression of complement related genes (*C3*, *C1s1*, *C3ar1*, and *F13a1*), suggesting a secondary effect of CERE-120 on the innate immunity after IR. There was also reduced expression of genes involved in extracellular matrix proteolysis (*Mmp2*, *Mmp3*, and *Cma1*). Interestingly, at this late stage (300 days) after IR and CERE-120 treatment, there were no DEGs directly related to parasympathetic or sympathetic function in the RNA-seq analysis; therefore, we screened genes that were DEGs after adenovirus-NRTN treatment at 60 days in our previous work.[8] While there were no significant changes in gene expression, there was variability in gene expression among SMGs. Genes such as *Vip*, *Adra2b*, *Vacht*, and *Tubb3* increased to a level similar to control levels with IR-CERE treatment (Figure S2A).

Interestingly, when we compared the RNA-seq data from non-IR with IR-CERE, there were even fewer DEGS, only 29, further suggesting that gene expression after CERE-120 treatment is more similar to non-IR glands (Table 3). There were 12 DEGs upregulated and 17 downregulated with IR-CERE treatment. However, most of these genes (21) were present in the list of non-IR versus IR-GFP (Table 1), suggesting they may be regulated by IR. Of the remaining 8 DEGs, most are ubiquitously expressed, and two of them, *Pdgfra* (platelet-derived growth factor receptor alpha) and *Dpt* (dermapontin), are differentially expressed in IR-GFP compared to IR-CERE.

In order to identify any pathways or general biological processes affected by the DEGs (Tables 1, 2, and 3), we used Gene Ontology (GO) analysis. We confirmed that the most prominently altered biological processes between non-IR and IR-GFP (72 DEGs) were the GO terms, Secretion (GO: 0046903), Synapses (GO: 0045202), Regulation of anatomical structure size (GO: 0090066), Regulation of cellular protein localization (GO: 1903827), and Intracellular transport (GO: 0046907) (Table 4), which is not surprising since gland hypofunction affects secretion, glandular innervation, and secretory protein localization and transport. However, the statistical analysis only showed false discovery rate (FDR) q values of 3.82×10^{-2}. What was more surprising was the GO analysis comparing IR-GFP with IR-CERE (38 DEGs, Table 4). GO analysis highlighted significant overlap of DEGs in GO terms such as Extracellular matrix (GO: 0031012), Collagen containing extracellular matrix (GO: 0062023), Leukocyte mediated immunity (GO: 0002443), Humoral immune response (GO: 0006959), Myeloid leukocyte mediated immunity (GO: 0002444), Secretory granule (GO: 0030141), Secretion (GO: 0046903), and Complement activation (GO: 0006956). In this case the GO lists had lower FDR q values ranging from 1.03×10^{-4} down to 8.41×10^{-10}. These GO terms suggest that IR-CERE treatment could influence fibrosis, the immune response within the gland, and secretion. There were significant overlaps with the immune response, particularly the reduction in IgG genes

Table 1. DEGs from RNA Sequencing Analysis of Murine SMGs: Non-IR versus IR-GFP Treatments

Gene	Log2 FC	adjusted p Value
Gm37795	−1.50	3.71E−05
Tef	−1.13	6.03E−05
Ccdc62	−1.24	6.03E−05
Rab27a	1.02	7.02E−05
Atp1a2	−1.71	7.57E−05
Il1rn	1.56	7.57E−05
Arl4a	0.64	4.86E−04
Zdhhc2	0.91	5.80E−04
Tbx3	0.80	7.48E−04
Senp3	−0.78	7.70E−04
Cpt1c	−1.44	1.30E−03
Gm6548	−1.10	1.49E−03
Amy1	2.25	1.95E−03
2010007H06Rik	−1.75	2.42E−03
Scrn1	1.73	2.60E−03
Clic6	1.17	3.41E−03
Mrfap1	0.68	4.28E−03
Dpysl3	0.67	4.49E−03
Spata13	0.81	5.38E−03
Tex2	0.88	5.38E−03
Vwf	1.28	6.81E−03
Dmxl2	−1.06	8.88E−03
Gm34314	1.79	8.88E−03
Ap4s1	0.64	9.90E−03
Nol9	−0.72	0.01
Scn3a	2.10	0.01
Sema3c	0.48	0.01
Ywhab	−0.68	0.01
Zfp263	−0.59	0.02
Bcl2l1	0.45	0.02
Kcnk5	0.65	0.02
Gucy1a1	−1.56	0.02
Baiap2l1	0.74	0.02
Csn3	−6.11	0.02
Rpl3	0.47	0.02
Trp53inp2	0.56	0.02
Brd3	−0.58	0.02
Edem1	0.80	0.03
Car8	1.03	0.03
Ccdc137	−0.54	0.03
Slc24a3	−0.97	0.03
Csnk1e	−0.88	0.03
Col23a1	−1.46	0.03
Mapk1ip1l	0.61	0.03
Tmcc1	−0.81	0.03
Zfp106	0.50	0.04
Slc16a6	0.68	0.04
Gm13648	0.92	0.04
Pls1	1.16	0.04
Sgms2	0.33	0.05
Dnajc3	0.49	0.05
Xpnpep3	0.95	0.05
Snap23	0.48	0.05
Atg14	−0.57	0.05
Prkcb	−1.84	0.05
Scgb2b10	−8.02	0.05
Kmt2a	−0.77	0.05
Tfap2b	0.74	0.05
Gpr37l1	1.34	0.05
Polr1b	−0.56	0.05
Per3	−1.17	0.05
Smgc	1.61	0.05
Zfp952	−0.57	0.05
Nol7	−0.54	0.05
mt-Co1	−0.56	0.05
8430436N08Rik	2.11	0.05
Gm28875	−0.57	0.05
Metap1	0.64	0.05
Galnt5	0.94	0.05
Atp13a2	−0.73	0.05
Rgl2	0.60	0.05
Agtr1a	1.66	0.05

(*Continued*)

Table 1. *Continued*

Data of each group was compared to one another. The lists of differentially expressed genes (DEGs) were generated after bioinformatic analysis of next-generation sequencing data and a cut-off at Log2 fold change (FC) and adjusted p values < 0.05. There were 72 DEGs comparing non-IR with IR-GFP.

and the humoral response as well as myeloid immunity and complement activation, which is part of the innate immunity. The GO analysis of the 29 DEGs in the non-IR versus IR-CERE group did not identify any significant GO terms(Table 4).

We also investigated protein expression comparing non-IR with IR-GFP and IR-CERE treatment. There was a clear decrease in the presence of protein SMGc, an embryonic mucin expressed in a subset of SMG proacinar cells[31] (Figures 3B and 3C), with IR-GFP and an increase with IR-CERE, which may reflect increased acinar differentiation with CERE-120 treatment. In addition, there was an increase in stromal MMP2 expression with IR-GFP, potentially involved in ECM remodeling associated with fibrosis after IR. The MMP2

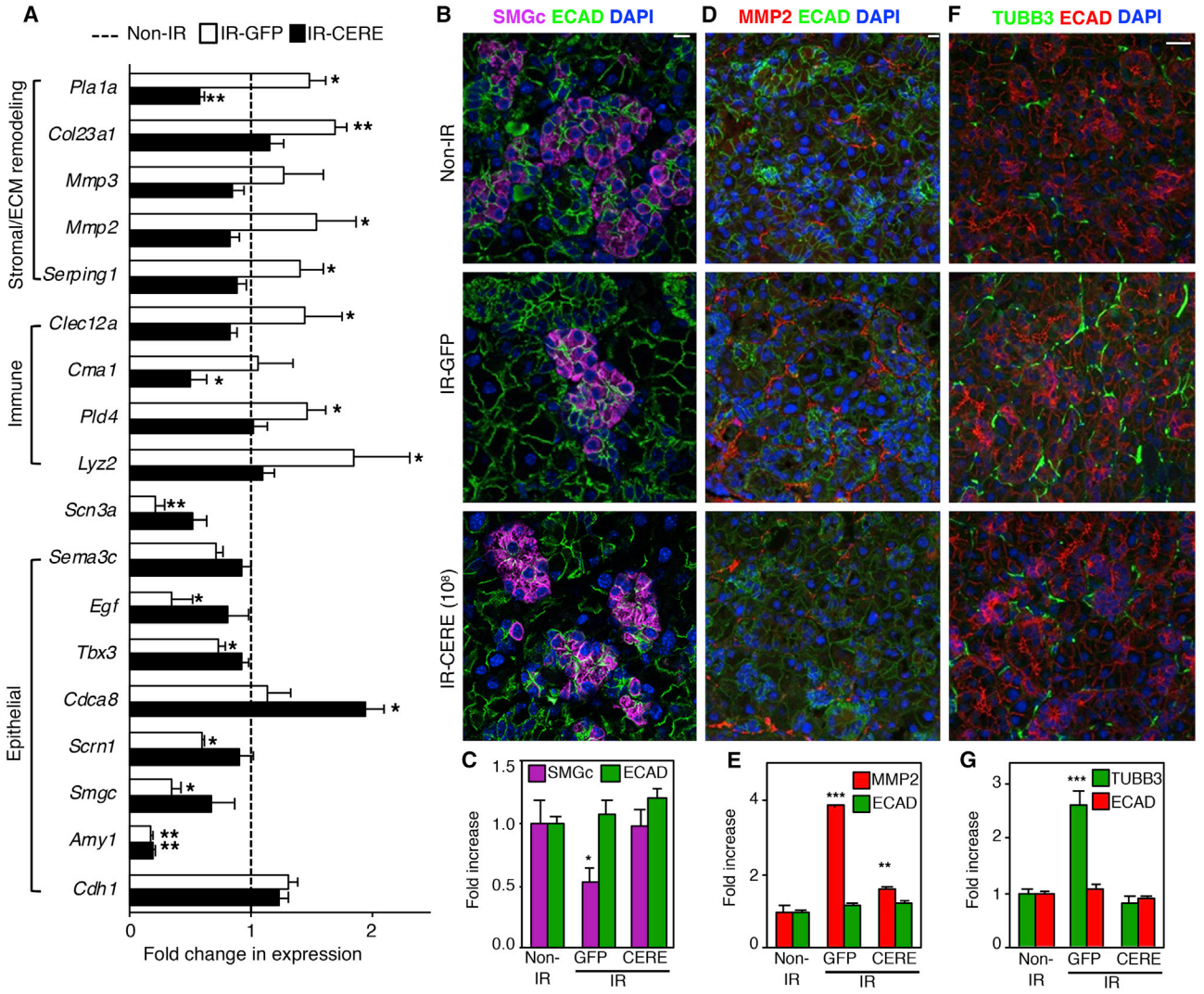

Figure 3. CERE-120 Treatment Reduces Levels of IR-Induced Fibrosis, Immune Response, and Innervation and Increases Proacinar Marker SMGc.
(A) Fold changes in gene expression of stromal/ECM remodeling, immune, and epithelial-related genes in AAV2-GFP (10^{10} vp/g) and CERE-120 (10^{8} vp/g) pre-IR treated glands. Data were normalized to *Gapdh* and non-IR glands (dotted line). Mean ± SEM, N > 3. ANOVA with *post hoc* Dunnett's test. **p < 0.01, *p < 0.05, as compared to non-IR. (B–G) Confocal imaging of SMGs of non-IR, AAV2-GFP 10^{10} vp/g, and CERE-120 10^{8} vp/g immunostained for (B) SMGc (magenta), E-cadherin (ECAD) (green), and nuclei (blue). Scale bar, 10 μm. (C) Quantification of SMGc and ECAD staining. (D) Immunostained for MMP2 (red), ECAD (green), and nuclei (blue). Scale bar, 20 μm. (E) Quantification of MMP2 and ECAD staining. (F) Immunostained for TUBB3-expressing neurons (green) and ECAD (red). (G) Quantification of TUBB3 and ECAD. All staining was normalized to the non-IR SMGs and nuclei. (C–G) Graphs show mean ± SEM. N > 3 glands with at least 5 images collected per gland. ANOVA with *post hoc* Dunnett's test. ***p < 0.001, **p < 0.01, *p < 0.05 compared to non-IR.

immunostaining was reduced in the IR-CERE treatment group (Figures 3D and 3E). Finally, there was an increase in the relative innervation of the gland after IR, as shown by tubulin3 (TUBB3) staining (Figures 3F and 3G). The increase of innervation after IR has been reported previously and may reflect a reduction of epithelium with IR combined with the survival of radiation-resistant nerves that appears as an increase in TUBB3 staining.[8] In sum, the RNA-seq analysis suggests that IR-CERE treatment results in gene expression patterns that reflect increased matrix remodeling and an improvement in homeostasis of both innate and humoral immunity.

Preclinical Porcine PG Studies of CERE-120 Treatment Pre-IR

We then tested CERE-120 treatment pre-IR using the PGs of the Yucatan minipig. We delivered AAV2-GFP or CERE-120 into the right-hand side PG of each animal via retrograde ductal injection. One week later, the AAV2-treated gland received a single dose of 15 Gy IR (Figure 4A), which has been used previously to induce chronic hyposalivation by 4 weeks post-IR.[20] Control groups consisted of AAV2-GFP (10^{9} vp/g) and CERE-120 (10^{9} vp/g) treatment of non-IR PGs, as well as AAV2-GFP (10^{12} vp/g) treatment a week before PG IR. Experimental treatment groups included IR-CERE in increasing doses (10^{8}, 10^{9}, 10^{10},

Table 2. DEGs from RNA Sequencing Analysis of Murine SMGs: IR-GFP versus IR-CERE Treatments

Gene	Log2 FC	adjusted p Value
Stromal		
Serping1	1.20	5.2E−07
Dpt	1.32	2.3E−06
C3	1.02	1.3E−03
Pla1a	1.95	4.0E−04
C1s1	1.10	4.2E−04
Pdgfra	1.03	2.9E−03
Dcn	0.69	4.7E−03
Mmp2	1.08	8.8E−03
Ccdc80	0.91	1.1E−02
Crispld2	0.88	1.4E−02
Mmp3	1.06	1.6E−02
Smoc2	0.75	4.3E−02
Adamts15	−0.72	1.6E−02
Immune		
C3ar1	1.09	1.2E−02
Lyz1	2.33	1.3E−02
Nfam1	0.94	1.5E−02
Clec12a	1.52	4.2E−02
Rab31	0.57	4.9E−02
Igkv8-19	3.86	4.2E−04
Igkv8-21	3.24	1.5E−03
Pld4	0.93	2.3E−03
Ighv1-5	2.97	2.5E−03
Igkv14-111	3.78	3.8E−03
Ighv2-9-1	4.40	4.0E−03
Igkv4-55	3.65	4.8E−03
Igkv4-61	3.49	1.3E−02
Ighg2c	2.43	4.3E−02
Ighv5-6	4.83	3.1E−02
Adgre1	1.38	5.4E−02
Cma1	1.96	5.5E−03
Lyz2	1.19	1.1E−02
Gm28875	0.57	1.6E−02
F13a1	0.87	1.7E−02
Scn2b	1.03	0.03
Other		
Cybrd1	1.16	4.72E−03
Cdca8	−1.11	3.02E−02
Scrn1	−1.33	0.03
Ddhd2	0.50	0.05

Data of each group was compared to one another. The lists of differentially expressed genes (DEGs) were generated after bioinformatic analysis of next-generation sequencing data and a cut-off at Log2 fold change (FC) and adjusted p values < 0.05. There were 38 DEGs comparing IR GFP with IR-CERE.

Table 3. DEGs from RNA Sequencing Analysis of Murine SMGs: Non-IR versus IR-CERE Treatments

Gene	log2 FC	p Value
Gm37795	−1.82	7.01E−09
Ccdc62	−1.30	8.60E−06
Ccdc137	−0.78	4.86E−05
Amy1	2.58	1.22E−04
Senp3	−0.80	7.49E−04
Chia1[a]	5.18	1.63E−03
Dpysl3	0.72	2.09E−03
Mrfap1	0.70	3.75E−03
Rpl3	0.54	3.75E−03
Dpt[a]	1.09	6.40E−03
Zdhhc2	0.80	6.91E−03
Sgms2	0.39	6.91E−03
Pdgfra[a]	1.08	9.85E−03
Zfp263	−0.60	0.01
Ralgds[a]	−0.67	0.01
Edem1	0.85	0.01
Zfp952	−0.66	0.01
Utp14a[a]	−0.53	0.01
Cpt1c	−1.25	0.01
Topbp1[a]	−0.73	0.02
Arl4a	0.51	0.02
Spata13[a]	0.74	0.02
Rab27a	0.73	0.02
Tef	−0.77	0.05
Pdia4[a]	0.42	0.05
Tex2	0.76	0.05
Gm13648	0.93	0.05
Gm6548	−0.87	0.05
Dnajc3	0.49	0.05

Data of each group was compared to one another. The lists of differentially expressed genes (DEGs) were generated after bioinformatic analysis of next-generation sequencing data and a cut-off at Log2 fold change (FC) and adjusted p values < 0.05. There were 29 DEGs comparing non-IR with IR-CERE.
[a]Genes not present in Table 1

10^{11}, and 10^{12} vp/g) delivered in 3 mL of sterile saline a week before IR. Every 2 weeks post-IR, pilocarpine-stimulated glandular saliva production was collected by cannulation of each PG (bilaterally), up to the 16 weeks conclusion of the experiment (Figure 4A). At the end of the experiment, the PGs were removed and a dramatic reduction in gland size and weight of all IR PGs was noted (Figure 4B), whereas the weight of the animals was not significantly different (Figure 4C). Compared to the non-IR groups treated with AAV2-GFP (G) or CERE-120 (CE), all IR glands regardless of the treatment showed significant decrease in gland weight (Figure 4D). Normalized gland weights (gland weight/animal weight) showed a similar result, except IR-CERE-120 10^{11} vg/g showed no difference compared to non-IR-GFP (Figure 4E).

Table 4. GO Pathway Analysis: Non-IR versus IR-GFP and IR-GFP versus IR-CERE Treatments

Gene Ontology Term	No. of Genes in Overlap	FDR q-value
Non-IR versus IR-GFP		
Secretion (GO: 0046903)	12	3.82E−02
Synapse (GO: 0045202)	10	3.82E−02
Regulation of anatomical structure size (GO: 0090066)	7	3.82E−02
Regulation of cellular protein localization (GO: 1903827)	7	3.82E−02
Intracellular transport (GO: 0046907)	12	3.82E−02
IR-GFP versus IR-CERE		
Extracellular matrix (GO: 0031012)	11	8.41E−10
Collagen containing extracellular matrix (GO: 0062023)	9	3.40E−08
Leukocyte mediated immunity (GO: 0002443)	12	3.30E−09
Humoral immune response (GO: 0006959)	8	1.78E−07
Myeloid leukocyte mediated immunity (GO: 0002444)	7	8.34E−05
Secretory granule (GO: 0030141)	11	3.40E−08
Secretion (GO: 0046903)	10	1.03E−04
Complement activation (GO: 0006956)	7	6.08E−08

GO pathway analysis of the gene lists from Tables 1, 2, and 3. The most highly significant GO terms were for the DEGs from Table 2, comparing IR-GFP with IR-CERE. There were no significant GO terms for the list of DEGs from non-IR and IR-CERE.

The contralateral non-treated PGs retained their normal weight as expected, since they did not receive IR or AAV2 vector (Figure 4F). There was variability among PG weights; for example, with IR-CERE-120, some PGs did increase in weight compared to IR-GFP (1 PG with 10^9 and 2 PGs with 10^{10} vg/g), although overall this was not significant. CERE-120 treatment increased NRTN protein expression, which was detected by immunostaining in clusters of cells of the IR PGs at 16 weeks post-treatment (Figure S3A). As expected, AAV2 viral particles were still detectable by qPCR in small biopsies of the PGs at the end of the experiment at 16 weeks and in murine SMGs after 300 days (Figures S3B and S3C), indicating that both AAV2-GFP and CERE-120 treatments persist for a prolonged time.

IR-Induced Alterations in Acinar Diameter and Ductal Marker Expression Are Restored by CERE-120 Treatment Pre-IR

Histological analysis of PGs stained with H&E and MT stain (Figures 5A and 5B) showed morphological changes with increased acinar size, similar to murine SMGs (Figure 2). For brevity, we only show images of IR-CERE 10^9 treatment. Furthermore, IR-CERE treatment had a beneficial effect and resulted in a more similar morphology to non-IR PGs (Figures 5A and 5B). Periductal and perivascular fibrosis was observed by MT staining with dark blue deposits of collagen-containing connective tissue in all treatment groups (Figure 5B). Interestingly, Keratin 19 (KRT19)-expressing ducts appeared to be smaller in size with fewer present in the IR-GFP-treated PGs compared to non-IR or IR-CERE treatment (Figures 5B and 5C). The tissue was dominated by enlarged acini structures that were easily observed with MT staining (Figure 5D, yellow Ac). These enlarged structures were also highlighted by enlarged luminal membranes and prominent areas of localization of the apical water channel aquaporin5 (AQP5) and E-cadherin (Figure 5E). Additionally, the acinar structures were highlighted by surrounding ACTA2-expressing myoepithelial cells (Figure 5F), and measurement of the acinus diameter showed that treatment with CERE-120 at 3 different doses reduced their size similar to the non-IR group (Figure 5G). Analysis of gene expression by qPCR was more variable in the porcine PG than murine SMG. This may be due to small biopsies to make cDNA from the large porcine PG that may not be representative of the entire gland, whereas the entire murine SMG is lysed for analysis. There is likely more regional variation in these small PG biopsies; for example, we avoided areas of the PG for biopsy where white spongy fibrotic fat was present, as RNA yields were negligible and of poor quality from these fibrotic biopsies (data not shown). Analysis of gene expression by qPCR of a few of the genes we had identified in the murine SMG were altered and showed a reduction in expression of acinar markers *AMY2* and *AQP5* with IR-GFP and an increase with IR-CERE treatment. In contrast, ductal markers such *KRT19* and *CFTR* increased with IR and reduced expression with IR-CERE treatment compared to non-IR-GFP-treated glands (Figure 5H). This highlights that the reduced KRT19 protein localization was associated with increased *KRT19* gene expression. Taken together, these data suggest that IR-induced changes in acinar morphology and gene expression are restored by CERE-120 treatment to levels similar to control in the porcine PG.

IR-Induced Alterations in Neuronal, Stromal, and Immune Cells Are Restored by CERE-120

We used immunostaining and qPCR analysis to investigate changes to the porcine PG nerves. We immunostained PGs with antibodies to TUBB3, which labels neurons; KRT19, which labels ducts that neurons are often associated with; and peanut lectin (PNA), which stains the basement membranes surrounding acinar structures. There was reduced TUBB3 staining with IR-GFP compared to their non-IR-GFP and IR-CERE treatments (Figure 6A, lower panels, and Figure 6B). This finding is in contrast to what happened in the murine SMGs, where there was an increase in neuronal staining (Figure 3F). In addition, IR PGs treated with CERE-120 had similar levels of staining for nerves within lobules of the gland, and lower doses (e.g., 10^9 vp/g) were similar to the non-IR group. Interestingly, hyperinnervation (i.e., thickened nerve bundles) were observed in periductal areas near large inter- and intra-lobular ducts with CERE-120 treatment (Figures S4A–S4D). There was also a reduction in KRT19 staining with CERE-120 10^{10-11} vp/g treatment. Quantitation of the PNA and KRT19 staining showed a reduction with IR-GFP and an increase to control levels with IR-CERE at lower doses. Analysis of gene expression of neuronal genes by qPCR showed that there was no change in expression of *TUBB3* message in any group. These data suggest that while CERE-120 increased neuronal staining after IR, there was an overall reduction in *TUBB3* mRNA levels. There was reduced expression of tyrosine hydroxylase (*TH*), a marker of the sympathetic

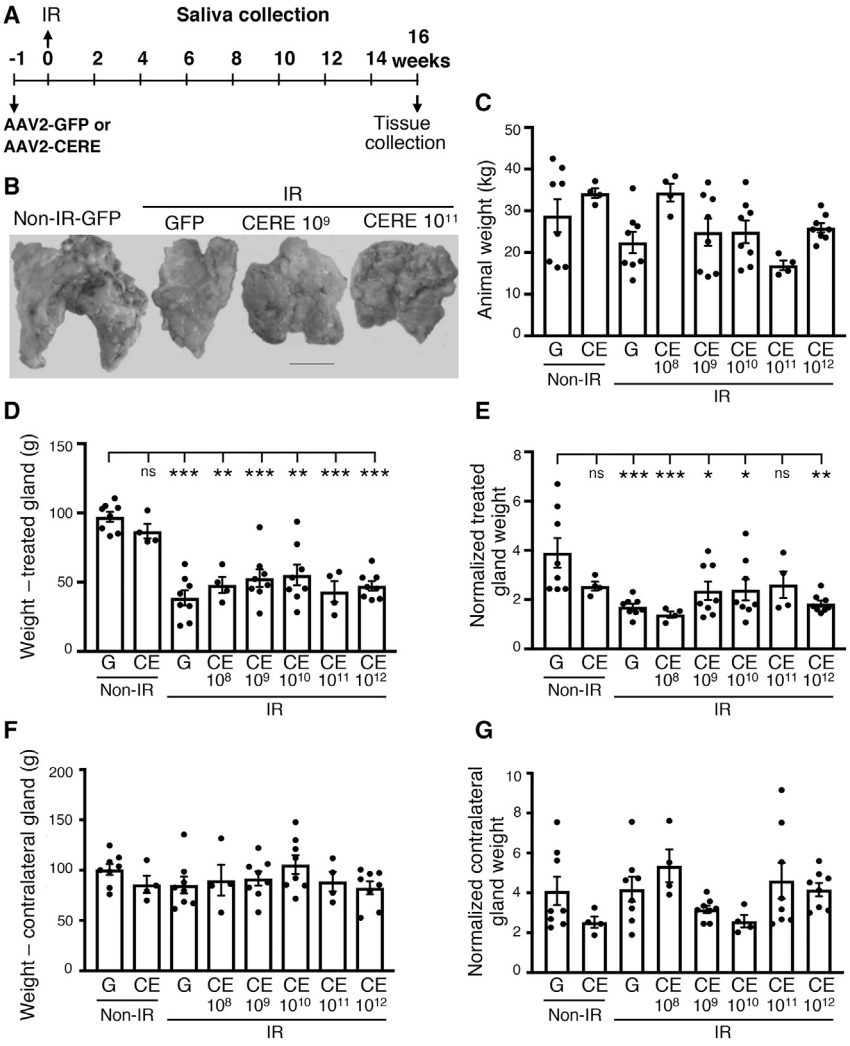

Figure 4. CERE-120 Treatment Pre-IR Does Not Increase the Weight of the IR PG, but the Contralateral Gland Is Similar to Non-IR Control.

(A) Schematic illustration of the study design with 52 animals. AAV2-GFP or CERE-120 gene therapy was delivered to one PG in each animal pre-IR. One week later, animals in the IR group received 15 Gy of radiation to the treated gland. Saliva was collected bi-weekly until 16 weeks, when tissues were harvested for analysis. (B) Representative images of the parotid salivary gland at the 16-week time point from various groups (non-IR-GFP, IR-GFP, and IR-CERE [10^9 and 10^{11}]). Scale bar, 5 cm. (C–G) Graphs representing animal weight (C), gland weight of the treated side (D), normalized treated gland weight (data from C/data from D) (E), gland weight of the contralateral non-treated side (F), and normalized contralateral non-treated gland weight (data from F/data from D) (G). Mean ± SEM. Dots represent data from individual animals. N > 4. ANOVA with *post hoc* Dunnett's test, ***p < 0.001, **p < 0.01, *p < 0.05, not significant (ns), as compared with non-IR-GFP.

nerves, although *GFRA2*, a marker of the parasympathetic nerves, was not reduced with IR, and both markers with CERE-120 treatment were similar to that of non-IR-GFP glands (Figure 6C).

We used qPCR to determine if IR-induced changes in markers of stromal/ECM remodeling and immune cells occurred in porcine PGs similar to murine SMGs (Figure 3A). We analyzed expression of some stromal and immune genes by qPCR; these included *SERPING1*, *LYZ* (the porcine version of *Lyz2* in the mouse), *MMP2*, and *C3*. Expression of *SERPING1*, *LYZ*, and *MMP2* was increased in IR-GFP PGs and was restored to levels comparable to that of non-IR-GFP glands with CERE-120 treatment (Figure 6C). Expression of *C3* did not increase with IR-GFP and remained similar to control levels with IR-CERE treatment. Since our GO analysis of murine SMGs had suggested that a significant number of genes associated with leukocyte immunity were altered, we immunostained the porcine PGs for CD45, a receptor-linked tyrosine phosphatase that is expressed on all leukocytes.[32] As expected, non-IR-GFP PGs showed staining of the occasional CD45+ leukocyte in the interstitial spaces around the acinar structures (Figure 6D). However, IR-GFP treatment increased CD45 staining (Figures 6D and 6E), which appeared in large fibroblast-like cells in the interstitial spaces. These cells may be CD45+ fibrocytes or macrophages, which may be responding to IR damage of the tissue or the fibrotic response. Thorough characterization of the porcine immune cells that respond to IR will be an important future research goal. The appearance of these cells was reduced with IR-CERE treatment, and the morphology of the CD45+ cells appeared similar to the non-IR-GFP group, suggesting immune homeostasis may have been restored (Figures 6D and 6E). Together, these data suggest that IR treatment reduces innervation of the porcine PG, reduces KRT19 duct cells, and increases markers of immune cells, all of which return to control levels after IR with the lower doses of CERE-120 treatment.

Low Doses of CERE-120 Prevent IR-Induced Hyposalivation in the Minipig

Over the 16 weeks of observation after CERE-120 treatment, the stimulated saliva volume of each gland (treated and contralateral) was measured in individual animals every 2 weeks. There was large variation with the stimulated saliva flow collected from an individual animal at each time point, so the volumes collected from 2–16 weeks were averaged and compared to baseline levels before IR (100%, dotted line) to generate summary graphs of the treated gland compared to the contralateral gland (Figures 7A and 7B). Non-IR-CERE-treated PGs showed similar saliva flow compared to non-IR-GFP-treated PGs (Figure 7A). As expected, IR-GFP-treated PGs

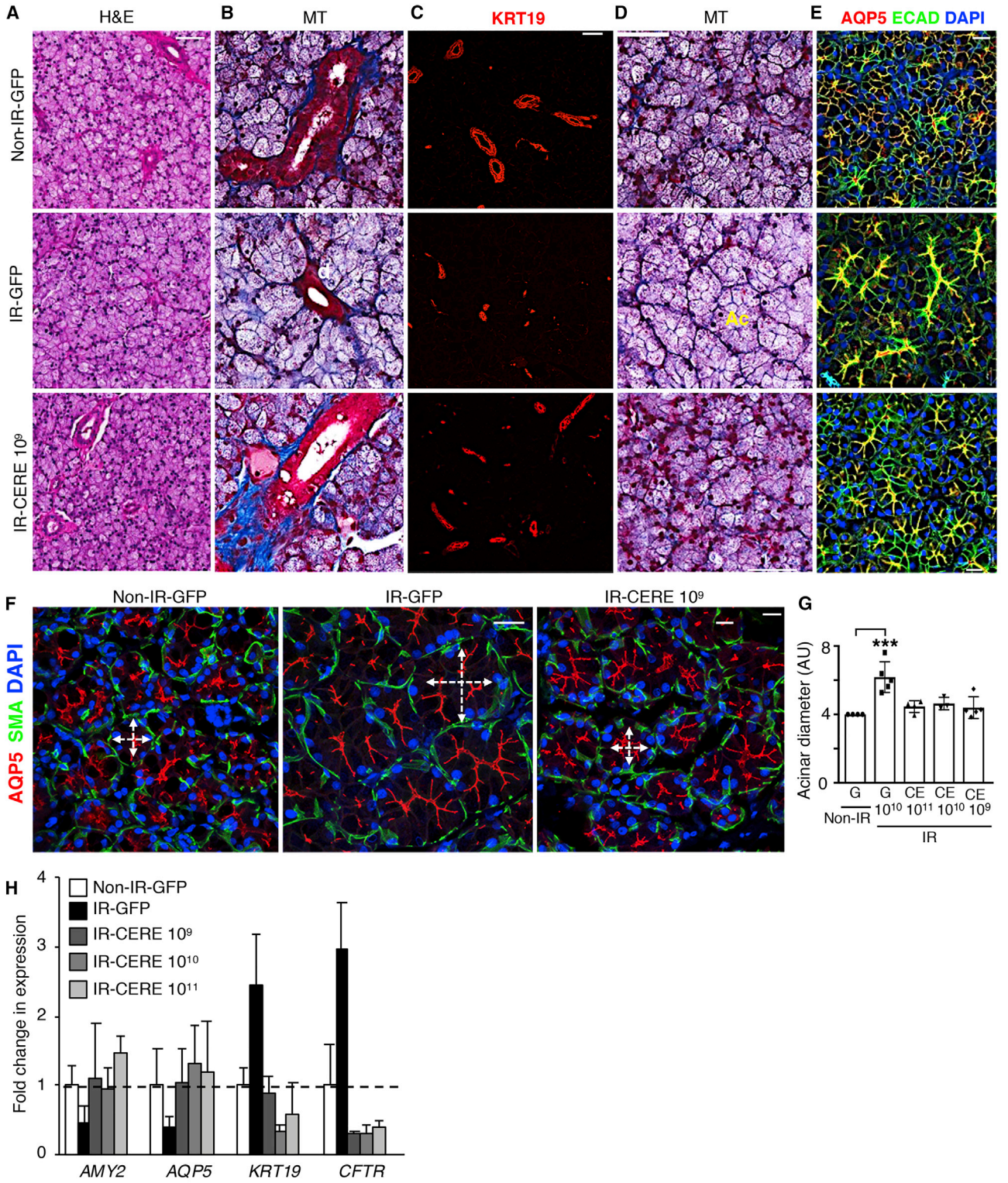

Figure 5. IR-Induced Alterations in Acinar Morphology and KRT19+ Ducts in Porcine PGs Are Prevented by CERE-120 Treatment before IR.

(A and B) Representative pictures of H&E and Masson trichrome (MT) staining on glands from various groups (non-IR-GFP, IR-GFP, and IR-CERE 10^9 groups). Scale bar, 50 μm. (C) Single 2 μm confocal sections of glands stained for Keratin 19 (red). Scale bar, 100 μm. (D) Pictures of MT staining showing enlarged acinar-tubular structures with

(legend continued on next page)

showed ~60%–65% reduction in saliva flow. Importantly, IR-CERE-treated PGs, in particular with the lower doses (10^8, 10^9, and 10^{10} vp/g), increased their average saliva flow, except for the 10^{11} vp/g group. It should be noted that some individual porcine PGs in the IR-CERE groups had similar saliva flow to the non-IR-GFP controls. While the contralateral gland did not receive any AAV2 vector or IR and were the same weight as non-IR-GFP PGs (Figure 4F), the saliva flow mimicked the pattern of the treated contralateral PG across all groups (Figure 7B). Due to the changes in saliva flow of the contralateral gland, we did not use the contralateral as control, instead averaging flow and comparing to the IR-GFP group.

To take a closer look at the temporal pattern of saliva flow in the treated and contralateral gland, we show the output of both glands within the animal groups over the 16-week experimental timeline. This highlights that with IR-GFP, the reduction in saliva flow begins within 2 weeks and is below 50% of baseline flow ($\leq$50% hyposalivation is shown as a gray shaded area with dotted line in each graph of Figure 7C) within 4 weeks and remained relatively stable over time (IR-GFP) (Figure 7C). The analysis also shows the individual variation of stimulated saliva flow at each time point and that non-IR-CERE results in over 200% of flow after 8 weeks. The highest dose of CERE-120 (10^{12}) did not show improved salivary flow at the end of the experiment, and saliva flow decreased over time. The CERE-120 (10^{11}) treatment did not improve saliva flow at any stage and appeared similar to IR-GFP. In contrast, the lower range of CERE-120 (10^8, 10^9, and 10^{10})-treated glands remained well above 50% of salivary flow (Figure 7C). Particularly after 16 weeks in the 10^8 and 10^9 groups, saliva flow showed similar values to those obtained from non-IR-GFP-treated glands. In conclusion, CERE-120 treatment before IR prevents the long-term effects of salivary hypofunction caused by IR and is most effective at low doses of viral delivery.

DISCUSSION

Here we show that retro-ductal infusion of CERE-120 into murine SMGs and porcine PGs prior to IR reduces the IR-induced salivary gland hypofunction and restores immune homeostasis. Analysis of murine SMGs 10 months after IR-CERE treatment showed there was reduced expression of many genes associated with the extracellular matrix and both the innate and adaptive humoral immune response. In porcine PGs, CERE-120 gene therapy improved salivary function and reduced the IR-induced alterations in acinar structure to control levels 16 weeks after IR. We confirmed there was also a reduction of IR-related immune response and fibrosis and an improvement of secretion with CERE-120 treatment in porcine PGs. Together, our results suggest CERE-120 may potentially be useful as gene therapy to prevent IR damage to salivary glands.

Previously, we showed NRTN treatment protected neuronal cells from apoptosis after IR-induced damage, and there was improved innervation, epithelial morphogenesis, and gene expression.[8,9,12] However, we had used recombinant NRTN protein or adenovirus-NRTN treatment for these studies, and their use in clinical settings is unlikely. Recombinant NRTN has a low solubility and short half-life,[33] and adenoviruses may elicit immune responses,[7] whereas AAV2 is considered safe and causes minimal inflammation.[23] Although cannulation is used clinically for imaging salivary glands during a sialogram, sub-acute areas of reversible inflammation can occur due to the procedure.[23]

In our murine studies, it is unclear whether the mechanism of action is different between the groups treated with vector before IR compared to after IR. Although pre-IR treatment was more effective at preventing hyposalivation at 90 days, the treatment after IR does show some striking positive effects in individual animals, although more variable at 120 and 300 days. The variability may potentially be caused by infusion of vector into a previously IR gland. Alternatively, post-IR treatment may take longer to reestablish epithelial-neuronal interactions and communication among radiation-surviving neuronal and immune cells. Taking into consideration that even the slightest increase in saliva production can translate in the subjective sensation of no longer having a dry mouth,[34] any increase in saliva flow above post-IR levels may clinically be perceived as beneficial for patients.

We then showed that CERE-120 treatment had similar effects on morphology and function in the porcine PGs. The AAV2 viral vector has been used for gene therapy because of its long-term persistence, and we detected AAV2 at the end of both murine and porcine experiments in salivary glands (Figures S3B and S3C). CERE-120 has been used for the potential treatment of Parkinson's disease,[35] and long-term safety of the vector in phase I/II clinical trials was shown up to 2 years.[15] Also, in Parkinson's-diseased rat brains, CERE-120 could be detected up to 18–20 months, and in monkeys up to 2 years, after a single treatment.[36] In these conditions, no antibodies against the NRTN protein were detected. Interestingly, the treatment of rat Parkinson's disease was equally effective in aged rats. It will be important to confirm the effects of CERE-120 on aged salivary glands, as there is a growing geriatric population suffering from head and neck cancer. It also remains to be determined whether the beneficial effects of CERE-120 affect secretory function of other exocrine and endocrine glands, such as lacrimal glands and pancreas.

A surprising finding in our porcine studies was that lower doses of virus (10^{8-10} vp/g) were as effective if not better than the higher doses to increase saliva flow, whereas in mice SMGs all three doses (10^6, 10^8, and 10^{10} vp/g) were similar in effect. With higher vector doses of

IR-GFP. Scale bar, 40 μm. (E) Confocal imaging of AQP5 (red), ECAD (green), and nuclei (blue) highlight the large luminal membranes of the enlarged acini structures. Scale bar, 20 μm. (F) Maximum intensity projections of confocal sections of glands stained for AQP5 (red), SMA (green), and nuclei (DAPI). Scale bar, 10 μm. Arrows indicate the diameter of an individual acinus. (G) Graph depicting the area of acinus diameter in glands from different treatment groups. Mean ± SEM. N > 3. ANOVA with *post hoc* Dunnett's test, ***p < 0.001, as compared to non-IR-GFP. (H) Gene expression of acinar and ductal-related markers. Mean ± SEM. N > 4. ANOVA with *post hoc* Dunnett's test compared to non-IR-GFP.

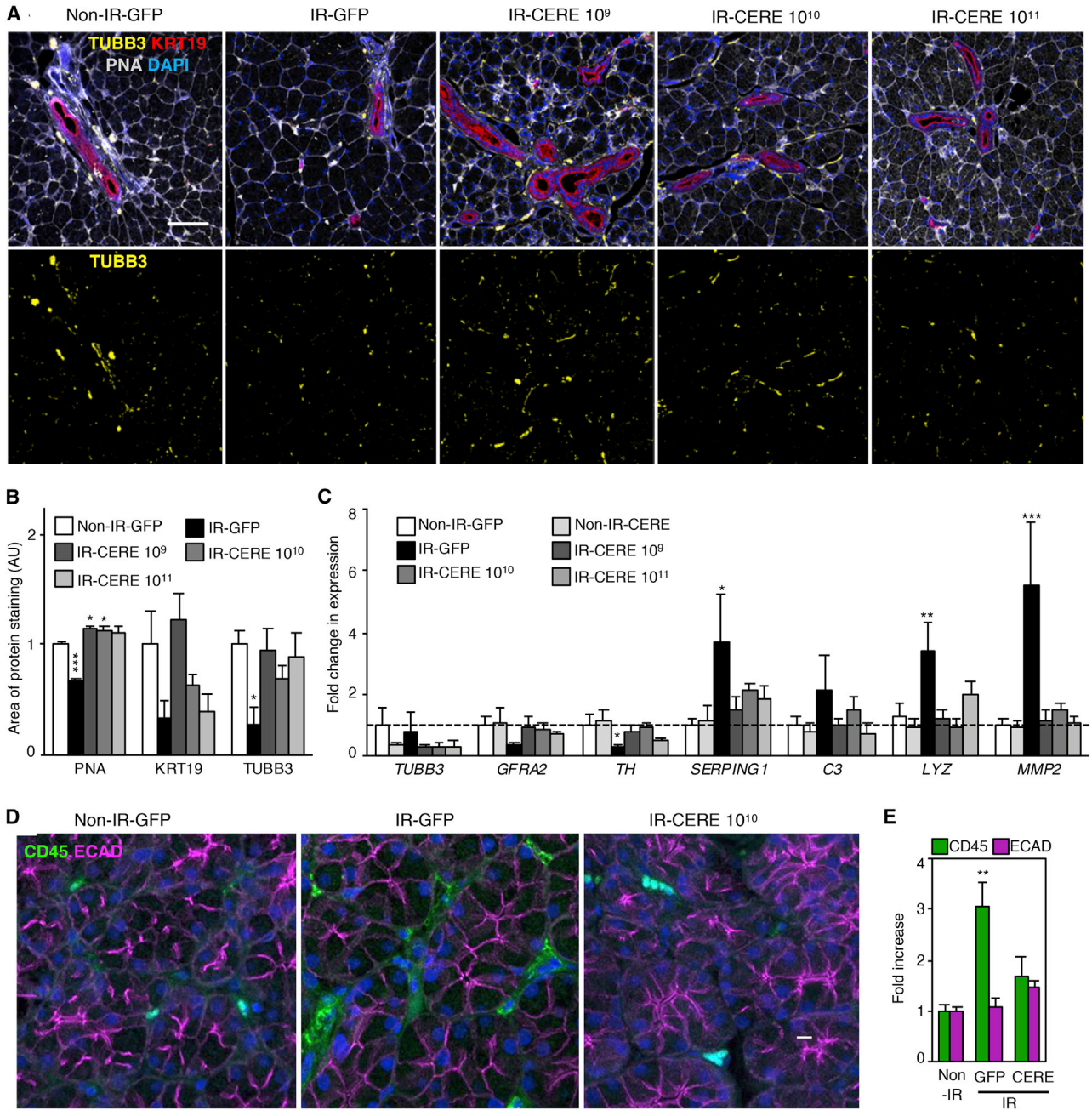

Figure 6. IR-Induced Changes in Neuronal, ECM Remodeling, and Immune Cells Are Restored by CERE-120 Treatment before IR in Minipigs.

(A) Representative confocal images of PGs from non-IR-GFP, IR-GFP, and IR-CERE (10^{11}, 10^{10}, and 10^{9} vp/g) stained for TUBB3 (yellow), KRT19 (red), Peanut Agglutinin (PNA) (gray), and nuclei (blue). The TUBB3 channel is shown in the lower panels for clarity. Scale bar, 100 μm. (B) Quantification of immunostaining showing fold increase in staining compared to non-IR-GFP. Graphs show mean ± SEM. N > 3 pigs with a minimum of 3 images collected per sample. ANOVA with *post hoc* Dunnett's test. ***p < 0.001, *p < 0.05 compared to non-IR-GFP. (C) Fold changes in gene expression of neuronal genes, *TUBB3*, *GFRA2*, and *TH*; genes involved in ECM remodeling and fibrosis, *SERPING1* and *MMP2*; and immune-related genes, *C3* and *LYZ*. Data were normalized to *RPS29* and non-IR glands (dotted line). Graphs show mean ± SEM. N > 3. ANOVA with *post hoc* Dunnett's test. ***p < 0.001, **p < 0.01, *p < 0.05 compared to non-IR. (D) Confocal images of PGs from non-IR-GFP, IR-GFP, and IR-CERE 10^{10} vp/g, stained for the leukocyte marker CD45 (green), ECAD (magenta), and nuclei (blue). Scale bar, 10 μm. (E) Quantification of CD45 normalized to the non-IR-GFP PGs. Graphs show mean ± SEM. N > 3. ANOVA with *post hoc* Dunnett's test. **p < 0.01 compared to non-IR.

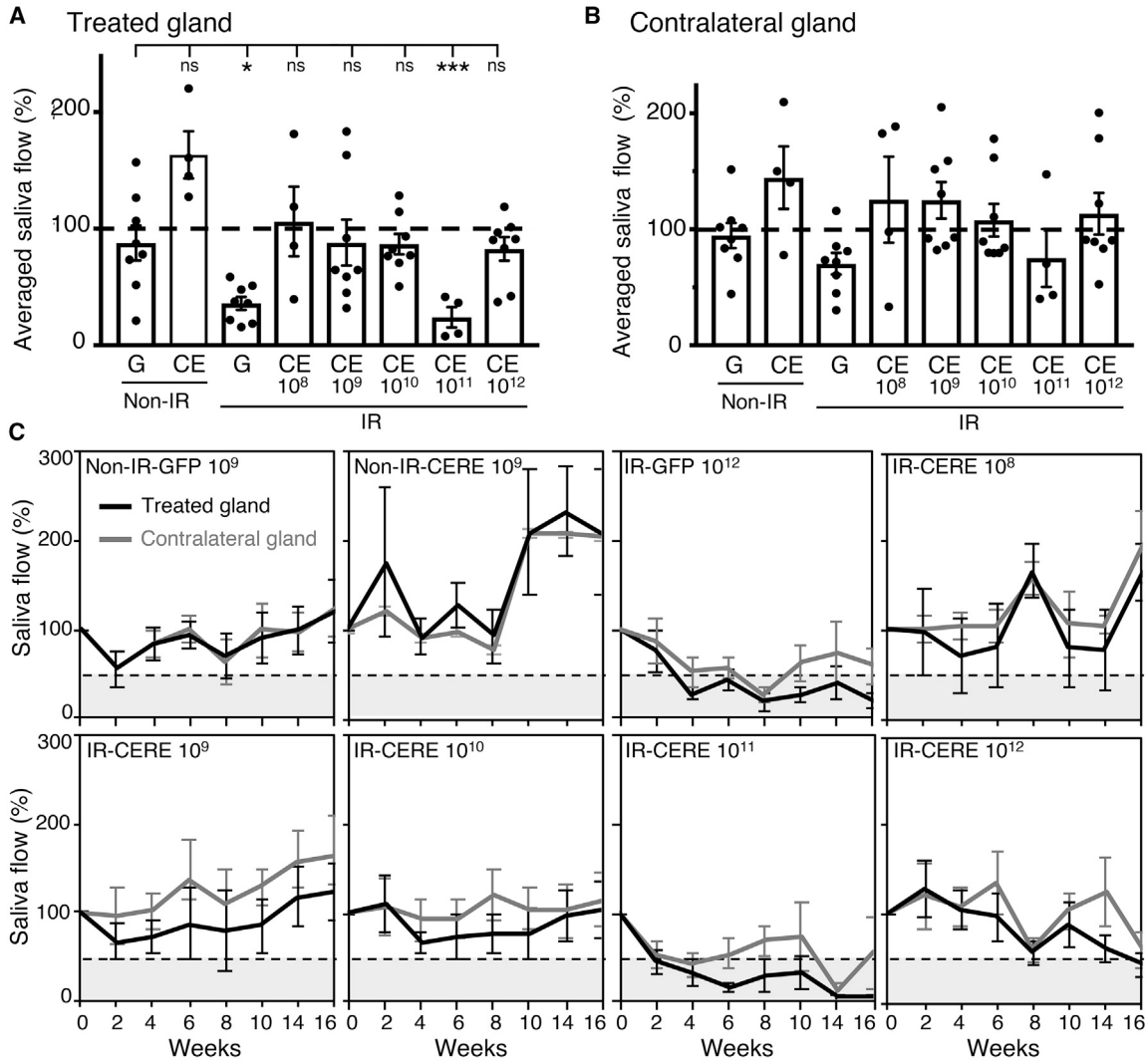

Figure 7. Low Doses of CERE-120 Gene Therapy Pre-IR Prevents IR-Induced Hyposalivation in Porcine PGs.

(A and B) Pilocarpine-stimulated saliva collected from the treated (A) and contralateral (B) parotid salivary gland was collected every 2 weeks. Saliva collected from 2–16 weeks was averaged and normalized to the baseline (dotted line, 100%). Mean ± SEM. N = 4–8 animals per group. ANOVA with *post hoc* Dunnett's test. *$p < 0.05$, ***$p < 0.001$, not significant (ns) when compared with non-IR-GFP group. (C) Time-course of saliva flow for various treatment groups. Black line, AAV2-treated gland. Gray line, non-IR non-treated contralateral gland. The gray area with dotted line represents ≤50% reduction in flow from baseline (100%). Mean ± SEM. N = 4–8 animals per group.

10^{11} and 10^{12} vp/g in porcine PGs, saliva flow decreased at 16 weeks to levels similar to the IR-GFP group (Figure 7C). Immunostaining and histology showed increased periductal hyperinnervation along the major ducts (Figure S4). Our previous *ex vivo* culture of fetal murine SMG also showed that high doses of recombinant NRTN in the media resulted in loss of epithelial innervation as the nerves extended past the gland and grew along the culture surface.[9] It is likely that very high levels of NRTN *in vivo* may not restore epithelial-neuronal homeostasis after IR.

Another interesting observation in minipigs was the coupled functional behavior of the contralateral and treated PGs within one animal, even though the weight (Figure 4F) and histology of the contralateral gland appears normal after IR. Previous reports showed that 16 weeks after IR there was a 60% reduction in the IR gland and a modest 17% reduction in flow of the contralateral gland.[19,21,37] Here, we quantitated the salivary flow of both glands for all groups. Surprisingly, CERE-120 treatment of a single non-IR PG increased saliva flow to a similar extent in both PGs, and generally any CERE-120 treatment resulted in similar trends in the salivary flow over time, whether up or down. There are a number of possible mechanisms. The coupled functional behavior may be due to central control of both PGs where regulatory feedback from one gland affects the other. Alternatively, a systemic secreted factor from a damaged gland or as a response to an improvement in

homeostasis may influence both glands' function. Our data also support a role for both the innate and the adaptive humoral immune system in the response to CERE-120, and this may be controlled by immune surveillance/function in both glands. Further investigation of potential neuronal immune function in response to CERE-120 and to both damage and repair is required.

NRTN is associated with inflammatory mechanisms in various mouse asthma models and may orchestrate inflammatory changes by linking the immune system with the nervous system in airway remodeling.[38,39] NRTN-deficient mice have increased T helper 2 (Th2) cytokine secretion, airway inflammation, and airway hyper-responsiveness and, when sensitized, showed increased collagen deposition and higher levels of neutrophils, matrix metalloproteinase 9 (MMP9), tumor necrosis factor alpha (TNF-α), and interleukin-6 (IL-6).[39] Furthermore, recombinant NRTN prior to the allergen challenge partially rescued the phenotype. Here, we show that IR increased expression of genes associated with the immune response, and CERE-120 treatment reduced expression to control levels (Figures 3 and 6). IR increased CD45 staining, which marks all the leukocytes, and large CD45+ cells, likely fibrocytes or macrophages, surrounded acinar cells in IR-GFP glands. The treatment with CERE-120 reduced the immune response, and the CD45+ cells appeared similar to those in non-IR-GFP PGs, suggesting a dampening of the immune response and a return to homeostasis.

Multiple approaches targeting different cellular mechanisms have been developed to treat IR-induced hyposalivation in minipigs, such as AQP1 and Shh gene therapy and rapamycin drug therapy.[3,17,19,20] Only AQP1 gene therapy has progressed to phase I/II clinical trials in humans.[6] In the future, combination therapies that target different mechanisms may be required to prevent and repair IR-induced injury. Here, we present a key translational advance using CERE-120 to prevent IR-induced hyposalivation in head and neck cancer patients. Low-dose CERE-120 gene therapy to human salivary glands before IR treatment may prevent and/or maintain function after IR by modulating communication among neuronal, immune, and epithelial cells to prevent saliva hypofunction and restore immune homeostasis of the remaining glandular tissue.

MATERIALS AND METHODS

AAV2 Vector Constructs

For all experiments we used the CERE-120 (AAV2-hNRTN) vector to administer human NRTN to salivary glands. The vector was produced by Sangamo BioSciences. A similar vector expressing GFP used as a control was purchased from Vector Biolabs (Cat# 7004).

In Vivo Mice Experiments

All murine experiments were approved by the National Institute of Dental and Craniofacial Research (NIDCR) Animal Care and Use Committee. Eight-week-old female C3H mice (National Cancer Institute Animal Production Area) were used. The treatment groups included injection of AAV2-GFP (10^{10} vp/g) or CERE-120 (10^6, 10^8, or 10^{10} vp/g) 10 days pre-IR or 60 days post-IR. Each group consisted of 5–10 mice. Baseline saliva (non-IR) was collected prior to vector delivery or IR. To irradiate the salivary glands, each animal was placed in a specially built Lucite jig. This jig immobilizes animals without the use of anesthetics and allows IR to the head and neck region only. Mice were irradiated in 5 fractions (6 Gy/day for 5 days) using a Therapax DXT300 X-ray irradiator (Pantak). After IR, animals were removed from the jig, housed (5 animals per cage) in a climate- and light-controlled environment, and allowed free access to food and water.

To deliver viral vectors into submandibular glands, mice were anesthetized with ketamine (60 mg/kg) and xylazine (8 mg/kg) intramuscularly, upon which vectors were delivered into both submandibular glands by retro-ductal infusion. During the cannulation, 0.5 mg/kg atropine was intramuscularly applied to inhibit saliva secretion in order to increase transduction efficiency.

For saliva collections, mice were anesthetized as mentioned above, followed by subcutaneous injection of pilocarpine at 0.25 mg/kg body weight to stimulate saliva secretion. Whole saliva was collected with a 75-mm hematocrit tube (Drummond) into 1.5 mL pre-weight Eppendorf tubes for 20 min and frozen immediately. After 10 months, mice were sacrificed in a carbon dioxide chamber and the glands were removed for analysis. Saliva was collected from the mice prior to the start of experiment (baseline/non-IR), at 90, 120, and 300 days.

Radiation of Porcine PGs

The Institutional Animal Care and Use Committee of Allegheny Singer Research Institute approved all animal experimentation described herein. As described in Wang et al.,[20] only one porcine PG was irradiated. Briefly, IR was delivered using a Siemens Primus linear accelerator (Concord, CA, USA). Animals were sedated and placed inside a vacuum form bag in the linear accelerator, and the PG was custom fitted using a Cerrobend (Bolton Metal Products, Bellefonte, PA, USA) to prevent the electron beam from hitting surrounding tissues. Digital radiography of the targeted (right) PG and non-targeted (left) parotid was adopted as previously described[20] to ensure irradiation to the targeted parotid and to confirm sparing of the contralateral parotid from radiation. A 12 MeV electron beam was used to deliver a single dose of 15 Gy to the gland. Following recovery from sedation, all pigs were returned to the husbandry unit.

Saliva Collection from Porcine PGs

Saliva from porcine PGs was collected as described in Wang et al.[20] All saliva was collected in the morning, bi-weekly and blindly. Minipigs were anaesthetized by intramuscular injection of a mixture of ketamine (20 mg/mL) and xylazine (2 mg/mL), placed on an operating table, and intubated in a prone position with a continuous infusion of isoflurane (1%–1.5%). An intramuscular injection of pilocarpine (1 mg/kg) was given to allow secretion of saliva. A 2 mL capacity oral swab (Salimetrics, Carlsbad, CA, USA) was weighed and placed covering the opening of the parotid Stensen's duct in the buccal corridor and mechanically secured. Saliva was collected by capillary action for 10 min, and the oral swab was replaced when needed.

The swabs were weighed, and saliva volume was calculated by subtracting the initial weight from the final weight.

Gene Delivery in the Porcine Model

This procedure was performed as previously described in Wang et al.[20] All gene transfer procedures were performed in the morning. The animals were sedated, intubated, and positioned supine for cannulation of the Stensen's duct. An intramuscular injection of 0.54 mg atropine was given, and after 10 min a P50 catheter fused to a P10 catheter was inserted into the opening of right-hand side Stensen's duct and secured with Vetbond (3M Products, St. Paul, MN, USA). CERE-120 or AAV2-GFP virus was infused into one gland of the animal (treated gland). All infusions were made in a 3 mL volume of sterile saline. The tubing was left in place for an additional 10 min to allow diffusion of the vector from the needle tip following infusion.

Tissue Processing and Histological Analysis of Murine SMGs and Porcine PGs

Salivary glands were dissected from the animals and weighed. For the porcine PGs, 0.5–1.5 cm^3 biopsies containing glandular tissue were collected from three separate regions of each gland, one close to the Stensen's duct, one in the middle part of the gland, and the other at edge of the gland. We avoided the abundant white fatty fibrotic tissue in the IR glands due to low RNA yields. All samples were analyzed individually, and the three biopsies were not pooled for immunohistochemistry (IHC) or RNA analysis purposes. Histological differences among the biopsies were observed by IHC analysis; for example, periductal regions were almost absent in samples taken at the edge of the gland. The location of small biopsies from the large PG may influence variability in qPCR data. The tissues were immediately fixed in 4% paraformaldehyde (PFA)/PBS, and the remaining gland was fixed in 20 volumes of formalin per weight of gland. The tissue biopsies were processed for conventional H&E and MT staining.

Immunostaining of Mouse and Porcine Salivary Glands

Paraffin-embedded tissue sections were analyzed for primary antibodies specific for smooth muscle actin (SMA) (Millipore Sigma, St. Louis, MO, USA, #A2547), AQP5 (Alomone, Jerusalem, Israel, #AQP-005), E-cadherin (Cell Signaling Technology, Boston, MA, USA, #3195), E-cadherin (BD Biosciences, San Jose, CA, USA, #610182), KRT19 (DSHB, IA, USA, TROMA III), Fluorescein-labeled Peanut Agglutinin (PNA) (Vector Laboratories, Burlingame, CA, USA, #FL-1071), Smgc (LSBio, #aa518-530 LC-C154825), Neuron-specific beta-III Tubulin (R&D, Tuj1#MAB1195), MMP2 (R&D, #AF1488), Neurturin (R&D, MN, USA, #AF477), and CD45 (Abcam, #ab23910).

Mouse or porcine glands were embedded in paraffin, sectioned onto slides (7 μm), dried at 60°C, and de-paraffinized in xylene substitute (Sigma, St. Louis, MO, USA) followed by re-hydration in graded ethanol solutions. Tissue sections were subjected to heat-mediated antigen retrieval using R-universal epitope recovery buffer (Electron Microscopy Sciences, Hatfield, PA, USA) for 10 min at high pressure. Sections were blocked for 1 h at room temperature with 10% heat-inactivated donkey serum (Jackson ImmunoResearch Laboratories, Westgrove, PA, USA), 1% BSA (Sigma, St. Louis, MO, USA), and Mouse on Mouse blocking reagent (Vector Laboratories, Burlingame, CA, USA). The slides were incubated overnight at 4°C with the appropriate primary antibody, then washed with PBS containing 0.1% Tween-20 (PBST) and incubated with the respective dye-conjugated secondary antibodies (all from Jackson ImmunoResearch Laboratories, Westgrove, PA, USA) and DAPI stain (EMD Millipore, Billerica, MA, USA) for 1 h at room temperature. Following washes with PBST, slides were mounted with Fluoro-Gel mounting medium (Electron Microscopy Sciences, Hatfield, PA, USA). All slides were imaged using the Zeiss 710 or 880 confocal microscopes. Images were thresholded to quantify the area of each protein staining, and the data were normalized to non-IR control. An average of five randomly selected areas of glandular tissue was taken per sample by a blinded observer and a minimum of three samples per group were combined and analyzed.

qPCR

Tissue samples for real-time PCR analysis were collected from three separate regions of the porcine PG and stored in RNAlater stabilizing solution (Ambion, Houston, TX, USA). Tissue (~25 mg) was homogenized in RNA lysis buffer using Fastprep-24 instrument with lysing matrix D (MP Biomedicals, Irvine, CA, USA). Murine SMGs were harvested, minced, and lyzed by homogenization. RNA was subsequently isolated using the RNAqueous-4PCR total RNA isolation kit and DNase reagents according to the manufacturer's instructions (Ambion, Houston, TX, USA). cDNA was generated from DNase-free RNA samples, amplified, and gene expression was normalized to the housekeeping gene *RPS*29 or *Gapdh* as previously described in Patel et al.[40]

RNA-Seq and Bioinformatics Analysis

cDNA libraries were produced from RNA of non-IR, pre-IR-GFP, and pre-IR-CERE (10^8) mouse submandibular glands using the Nextera XT method. Samples were run on an Illumina NextSeq500 configured for 37 paired-end (PE) reads. FASTQ files were extracted using bcl2fastq, and the FASTQ files were further processed using the *snakemake/3.8* utility in the Biowulf2 cluster. Quality of the reads was evaluated using the FastQC software. Read mapping against a recent ENCODE mouse release was performed using the STAR v2.5.2a aligner using the standard mode with mapping parameters derived from the GENCODE project. Subsequently, the quality of the mapping was analyzed using the QoRTs_QC package, which generates multiple statistics about the quality of the mapping and the samples. DeSeq2 was used to performed statistical test analysis to assess differential gene expression (DGE) between groups with a log2 fold in expression with the adjusted p value of <0.05, as previously described in Athwal et al.[41] RNA-seq data are available on the Gene Expression Omnibus (GEO) website (GEO: GSE150112).

TaqMan PCR to Quantify AAV2 Vector Level in Salivary Gland Tissues

To evaluate the AAV2 genome levels, tissue samples were analyzed using real-time qPCR and TaqMan chemistry. Genomic DNA from frozen tissue samples was extracted using DNeasy Blood & Tissue

kit (QIAGEN, Valencia, CA, USA). Two different sets of primers and probes were used to measure the viral particles in genomic DNA. As previously reported, primers detecting AAV2 ITR were used:[42] the forward ITR primer (5′-GGAACCCCTAGTGATG GAGTT-3′) and the reverse ITR primer (5′-CGGCCTCAGT GAGCGA-3′). The hydrolysis probe was labeled with fluorescein (FAM) and quenched with BlackBerry quencher (BBQ) (AAV2 ITR probe, 5′-FAM-CACTCCCTCTCTGCGCGCTCG-BBQ-3′). Another probe set was also designed using Beacon Designer software (PREMIER Biosoft International, Palo Alto, CA, USA) to detect the CMV enhancer in the AAV2 vector. The forward CMV primer 5′-GGAGTATTTACGGTAAACTG-3′, the reverse CMV primer 5′-GTCCCATAAGGTCATGTA-3′, and the hydrolysis probe were labeled with FAM on the 5′ end and quenched with QSY on the 3′ end (AAV2 CMV probe, 5′-FAM-CAAGTGTATCA TATGCCAAGTACGCC-QSY-3′). Primers, probe, and oligonucleotides were synthesized by Thermofisher (Waltham, MA USA).

qPCR was performed with the CFX96 Real-Time PCR detection system (BIORAD, Hercules, CA, USA). PCRs were performed in a 25 μL final volume using TaqMan Universal PCR Master Mix (Applied Biosystems, Waltham, MA, USA) supplemented with 1 μM each of primers and probes and 10 μL of template DNA (either plasmid standard or extracted sample DNA). The PCR profile contained a uracil-N-glycosylase (UNG) treatment at 50°C for 2 min, an initial denaturation step at 95°C for 10 min, followed by 40 cycles of denaturation at 95°C for 30 s and 60°C for 1 min. Each qPCR run was controlled by a "No template" negative control performed in triplicate. As a positive control, and calculation of the standard curves, eight serial dilutions of the plasmid standard pAc CMV pLAc (containing 10^1–10^8 plasmid copies per 10 μL) were prepared and subjected to qPCR analysis in triplicate. Data analysis was performed with CFX Maestro software (BIORAD, Hercules, CA, USA) to generate the standard curves and to determine the concentration of AAV2 in the DNA samples by interpolation. To analyze the influence of genomic DNA on the robustness of our PCR, defined numbers of plasmid DNA molecules were spiked with various amounts of genomic DNA extracted from non-IR salivary gland DNA.

Statistical Analysis

Values are expressed as mean ± standard error of the mean (SEM). Data were log transformed and analyzed with an unpaired Student's t test (two-tailed) for comparing two groups or a one-way ANOVA with Dunnett's multiple comparisons test for more than two groups. Treatment groups were compared to the non-IR control (mouse experiments) or non-IR-GFP (porcine experiments) using Prism 8.4 software (GraphPad, La Jolla, CA, USA). Tables of DEGs were generated using the DESeq2 package and the Wald test with Benjamini-Hochberg adjusted p values < 0.05 and Log2 fold change.

SUPPLEMENTAL INFORMATION

Supplemental Information can be found online at https://doi.org/10.1016/j.omtm.2020.07.016.

AUTHOR CONTRIBUTIONS

Conceptualization, M.P.H., I.M.A.L., and M.J.P.; Methodology, M.P.H., M.J.P., and J.A.C.; Investigation, V.N.P., C.E.J., D.C.V., A.E.C., M.R.M., E.B., C.Z., C.M.G., L.Z., M.T., and P.C.E.; Resources, K.M., D.A., M.J.P., and J.A.C.; Data Curation, D.M., V.N.P., and M.P.H.; Writing- Review and Editing, I.M.A.L., V.N.P., and M.P.H.; Visualization, V.N.P. and M.P.H.; Supervision, M.P.H., I.M.A.L., M.J.P., and V.N.P.; Funding Acquisition, M.P.H.

CONFLICTS OF INTEREST

The authors declare no competing interests.

ACKNOWLEDGMENTS

We would like to thank the NIH Genomic and Computational Biology Core (ZIC DC000086) for preparing the RNA sequencing (RNA-seq) libraries and performing RNA-seq analysis, the NIDCR Imaging Core for help with imaging analysis (ZIC DE000750-01), and the NIDCR Veterinary Resources Core for assistance with the murine procedures (ZIC DE000740-05). We would also like to thank the veterinary core at Allegheny General Hospital for assistance with the porcine procedures. We would like to thank Dr. Marit H. Aure and Dr. Augustin Chibly for their helpful discussions and assistance with submandibular gland (SMG) dissections. This project was funded in part by the Intramural Program of the NIH at NIDCR, Bethesda, MD, USA (ZIA DE000722 to M.P.H., ZIA DE000695 to J.A.C.), and by NIH grants R21DE028690 (to I.M.L.) and R01DE022973 (to M.J.P.).

REFERENCES

1. Vissink, A., Mitchell, J.B., Baum, B.J., Limesand, K.H., Jensen, S.B., Fox, P.C., Elting, L.S., Langendijk, J.A., Coppes, R.P., and Reyland, M.E. (2010). Clinical management of salivary gland hypofunction and xerostomia in head-and-neck cancer patients: successes and barriers. Int. J. Radiat. Oncol. Biol. Phys. *78*, 983–991.

2. Morgan-Bathke, M., Harris, Z.I., Arnett, D.G., Klein, R.R., Burd, R., Ann, D.K., and Limesand, K.H. (2014). The Rapalogue, CCI-779, improves salivary gland function following radiation. PLoS ONE *9*, e113183.

3. Zhu, Z., Pang, B., Iglesias-Bartolome, R., Wu, X., Hu, L., Zhang, C., Wang, J., Gutkind, J.S., and Wang, S. (2016). Prevention of irradiation-induced salivary hypofunction by rapamycin in swine parotid glands. Oncotarget *7*, 20271–20281.

4. Lombaert, I.M., Movahednia, M.M., Adine, C., and Ferreira, J.N. (2016). Concise Review: Salivary Gland Regeneration: Therapeutic Approaches from Stem Cells to Tissue Organoids. Stem Cells *35*, 97–105.

5. Ozdemir, T., Fowler, E.W., Hao, Y., Ravikrishnan, A., Harrington, D.A., Witt, R.L., Farach-Carson, M.C., Pradhan-Bhatt, S., and Jia, X. (2016). Biomaterials-based strategies for salivary gland tissue regeneration. Biomater. Sci. *4*, 592–604.

6. Alevizos, I., Zheng, C., Cotrim, A.P., Liu, S., McCullagh, L., Billings, M.E., Goldsmith, C.M., Tandon, M., Helmerhorst, E.J., Catalán, M.A., et al. (2017). Late responses to adenoviral-mediated transfer of the aquaporin-1 gene for radiation-induced salivary hypofunction. Gene Ther. *24*, 176–186.

7. Baum, B.J., Alevizos, I., Zheng, C., Cotrim, A.P., Liu, S., McCullagh, L., Goldsmith, C.M., Burbelo, P.D., Citrin, D.E., Mitchell, J.B., et al. (2012). Early responses to adenoviral-mediated transfer of the aquaporin-1 cDNA for radiation-induced salivary hypofunction. Proc. Natl. Acad. Sci. USA *109*, 19403–19407.

8. Ferreira, J.N.A., Zheng, C., Lombaert, I.M.A., Goldsmith, C.M., Cotrim, A.P., Symonds, J.M., Patel, V.N., and Hoffman, M.P. (2018). Neurturin Gene Therapy Protects Parasympathetic Function to Prevent Irradiation-Induced Murine Salivary Gland Hypofunction. Mol. Ther. Methods Clin. Dev. *9*, 172–180.

9. Knox, S.M., Lombaert, I.M., Haddox, C.L., Abrams, S.R., Cotrim, A., Wilson, A.J., and Hoffman, M.P. (2013). Parasympathetic stimulation improves epithelial organ regeneration. Nat. Commun. *4*, 1494.

10. Knox, S.M., Lombaert, I.M., Reed, X., Vitale-Cross, L., Gutkind, J.S., and Hoffman, M.P. (2010). Parasympathetic innervation maintains epithelial progenitor cells during salivary organogenesis. Science *329*, 1645–1647.

11. Vining, K.H., Lombaert, I.M.A., Patel, V.N., Kibbey, S.E., Pradhan-Bhatt, S., Witt, R.L., and Hoffman, M.P. (2019). Neurturin-containing laminin matrices support innervated branching epithelium from adult epithelial salispheres. Biomaterials *216*, 119245.

12. Lombaert, I.M., Abrams, S.R., Li, L., Eswarakumar, V.P., Sethi, A.J., Witt, R.L., and Hoffman, M.P. (2013). Combined KIT and FGFR2b signaling regulates epithelial progenitor expansion during organogenesis. Stem Cell Reports *1*, 604–619.

13. Heuckeroth, R.O., Enomoto, H., Grider, J.R., Golden, J.P., Hanke, J.A., Jackman, A., Molliver, D.C., Bardgett, M.E., Snider, W.D., Johnson, E.M., Jr., and Milbrandt, J. (1999). Gene targeting reveals a critical role for neurturin in the development and maintenance of enteric, sensory, and parasympathetic neurons. Neuron *22*, 253–263.

14. Rossi, J., Luukko, K., Poteryaev, D., Laurikainen, A., Sun, Y.F., Laakso, T., Eerikäinen, S., Tuominen, R., Lakso, M., Rauvala, H., et al. (1999). Retarded growth and deficits in the enteric and parasympathetic nervous system in mice lacking GFR alpha2, a functional neurturin receptor. Neuron *22*, 243–252.

15. Marks, W.J., Jr., Baumann, T.L., and Bartus, R.T. (2016). Long-Term Safety of Patients with Parkinson's Disease Receiving rAAV2-Neurturin (CERE-120) Gene Transfer. Hum. Gene Ther. *27*, 522–527.

16. Marks, W.J., Jr., Ostrem, J.L., Verhagen, L., Starr, P.A., Larson, P.S., Bakay, R.A., Taylor, R., Cahn-Weiner, D.A., Stoessl, A.J., Olanow, C.W., and Bartus, R.T. (2008). Safety and tolerability of intraputaminal delivery of CERE-120 (adeno-associated virus serotype 2-neurturin) to patients with idiopathic Parkinson's disease: an open-label, phase I trial. Lancet Neurol. *7*, 400–408.

17. Hu, L., Zhu, Z., Hai, B., Chang, S., Ma, L., Xu, Y., Li, X., Feng, X., Wu, X., Zhao, Q., et al. (2018). Intragland Shh gene delivery mitigated irradiation-induced hyposalivation in a miniature pig model. Theranostics *8*, 4321–4331.

18. Ma, C., Fan, Z., Gao, Z., Wang, S., and Shan, Z. (2017). Delivery of human erythropoietin gene with an adeno-associated virus vector through parotid glands to treat renal anaemia in a swine model. Gene Ther. *24*, 692–698.

19. Shan, Z., Li, J., Zheng, C., Liu, X., Fan, Z., Zhang, C., Goldsmith, C.M., Wellner, R.B., Baum, B.J., and Wang, S. (2005). Increased fluid secretion after adenoviral-mediated transfer of the human aquaporin-1 cDNA to irradiated miniature pig parotid glands. Mol. Ther. *11*, 444–451.

20. Wang, Z., Zourelias, L., Wu, C., Edwards, P.C., Trombetta, M., and Passineau, M.J. (2015). Ultrasound-assisted nonviral gene transfer of AQP1 to the irradiated minipig parotid gland restores fluid secretion. Gene Ther. *22*, 739–749.

21. Li, J., Shan, Z., Ou, G., Liu, X., Zhang, C., Baum, B.J., and Wang, S. (2005). Structural and functional characteristics of irradiation damage to parotid glands in the miniature pig. Int. J. Radiat. Oncol. Biol. Phys. *62*, 1510–1516.

22. Voutetakis, A., Kok, M.R., Zheng, C., Bossis, I., Wang, J., Cotrim, A.P., Marracino, N., Goldsmith, C.M., Chiorini, J.A., Loh, Y.P., et al. (2004). Reengineered salivary glands are stable endogenous bioreactors for systemic gene therapeutics. Proc. Natl. Acad. Sci. USA *101*, 3053–3058.

23. Zheng, C., Voutetakis, A., Goldstein, B., Afione, S., Rivera, V.M., Clackson, T., Wenk, M.L., Boyle, M., Nyska, A., Chiorini, J.A., et al. (2011). Assessment of the safety and biodistribution of a regulated AAV2 gene transfer vector after delivery to murine submandibular glands. Toxicol. Sci. *123*, 247–255.

24. Liu, X., Cotrim, A., Teos, L., Zheng, C., Swaim, W., Mitchell, J., Mori, Y., and Ambudkar, I. (2013). Loss of TRPM2 function protects against irradiation-induced salivary gland dysfunction. Nat. Commun. *4*, 1515.

25. O'Connell, A.C., Redman, R.S., Evans, R.L., and Ambudkar, I.S. (1999). Radiation-induced progressive decrease in fluid secretion in rat submandibular glands is related to decreased acinar volume and not impaired calcium signaling. Radiat. Res. *151*, 150–158.

26. Teos, L.Y., Zheng, C.Y., Liu, X., Swaim, W.D., Goldsmith, C.M., Cotrim, A.P., Baum, B.J., and Ambudkar, I.S. (2016). Adenovirus-mediated hAQP1 expression in irradiated mouse salivary glands causes recovery of saliva secretion by enhancing acinar cell volume decrease. Gene Ther. *23*, 572–579.

27. Giannandrea, M., and Parks, W.C. (2014). Diverse functions of matrix metalloproteinases during fibrosis. Dis. Model. Mech. *7*, 193–203.

28. Gettins, P.G. (2002). Serpin structure, mechanism, and function. Chem. Rev. *102*, 4751–4804.

29. Wang, X.L., Hou, L., Zhao, C.G., Tang, Y., Zhang, B., Zhao, J.Y., and Wu, Y.B. (2019). Screening of genes involved in epithelial-mesenchymal transition and differential expression of complement-related genes induced by PAX2 in renal tubules. Nephrology (Carlton) *24*, 263–271.

30. Inoue, A., Arima, N., Ishiguro, J., Prestwich, G.D., Arai, H., and Aoki, J. (2011). LPA-producing enzyme PA-PLA$_1\alpha$ regulates hair follicle development by modulating EGFR signalling. EMBO J. *30*, 4248–4260.

31. Das, B., Cash, M.N., Hand, A.R., Shivazad, A., Grieshaber, S.S., Robinson, B., and Culp, D.J. (2010). Tissue distibution of murine Muc19/smgc gene products. J. Histochem. Cytochem. *58*, 141–156.

32. Altin, J.G., and Sloan, E.K. (1997). The role of CD45 and CD45-associated molecules in T cell activation. Immunol. Cell Biol. *75*, 430–445.

33. Paul, G., and Sullivan, A.M. (2019). Trophic factors for Parkinson's disease: Where are we and where do we go from here? Eur. J. Neurosci. *49*, 440–452.

34. Fox, P.C., Busch, K.A., and Baum, B.J. (1987). Subjective reports of xerostomia and objective measures of salivary gland performance. J. Am. Dent. Assoc. *115*, 581–584.

35. Hickey, P., and Stacy, M. (2013). AAV2-neurturin (CERE-120) for Parkinson's disease. Expert Opin. Biol. Ther. *13*, 137–145.

36. Herzog, C.D., Bishop, K.M., Brown, L., Wilson, A., Kordower, J.H., and Bartus, R.T. (2011). Gene transfer provides a practical means for safe, long-term, targeted delivery of biologically active neurotrophic factor proteins for neurodegenerative diseases. Drug Deliv. Transl. Res. *1*, 361–382.

37. Gao, R., Yan, X., Zheng, C., Goldsmith, C.M., Afione, S., Hai, B., Xu, J., Zhou, J., Zhang, C., Chiorini, J.A., et al. (2011). AAV2-mediated transfer of the human aquaporin-1 cDNA restores fluid secretion from irradiated miniature pig parotid glands. Gene Ther. *18*, 38–42.

38. Mauffray, M., Domingues, O., Hentges, F., Zimmer, J., Hanau, D., and Michel, T. (2015). Neurturin influences inflammatory responses and airway remodeling in different mouse asthma models. J. Immunol. *194*, 1423–1433.

39. Michel, T., Thérésine, M., Poli, A., Domingues, O., Ammerlaan, W., Brons, N.H., Hentges, F., and Zimmer, J. (2011). Increased Th2 cytokine secretion, eosinophilic airway inflammation, and airway hyperresponsiveness in neurturin-deficient mice. J. Immunol. *186*, 6497–6504.

40. Patel, V.N., Likar, K.M., Zisman-Rozen, S., Cowherd, S.N., Lassiter, K.S., Sher, I., Yates, E.A., Turnbull, J.E., Ron, D., and Hoffman, M.P. (2008). Specific heparan sulfate structures modulate FGF10-mediated submandibular gland epithelial morphogenesis and differentiation. J. Biol. Chem. *283*, 9308–9317.

41. Athwal, H.K., Murphy, G., 3rd, Tibbs, E., Cornett, A., Hill, E., Berenstein, E., Hoffman, M.P., and Lombaert, I.M.A. (2019). SOX10 regulates plasticity in the formation of secretory units of exocrine glands. Stem Cell Reports *12*, 366–380.

42. Aurnhammer, C., Haase, M., Muether, N., Hausl, M., Rauschhuber, C., Huber, I., Nitschko, H., Busch, U., Sing, A., Ehrhardt, A., and Baiker, A. (2012). Universal real-time PCR for the detection and quantification of adeno-associated virus serotype 2-derived inverted terminal repeat sequences. Hum. Gene Ther. Methods *23*, 18–28.